Reduction of the spherical aberration effect in high-numerical-aperture optical scanning instruments

Isabel Escobar, Genaro Saavedra, and Manuel Martínez-Corral

Departamento de Óptica, Universidad de Valencia, E46100 Burjassot, Spain

Jesús Lancis

Departament de Ciències Experimentals, Universitat Jaume I, 12080 Castelló, Spain

Received March 17, 2006; revised June 15, 2006; accepted June 16, 2006; posted July 5, 2006 (Doc. ID 69042)

In modern high-numerical-aperture (NA) optical scanning instruments, such as scanning microscopes, optical data storage systems, or laser trapping technology, the beam emerging from the high-NA objective focuses deeply through an interface between two media of different refractive index. Such a refractive index mismatch introduces an important amount of spherical aberration, which increases dynamically when scanning at increasing depths. This effect strongly degrades the instrument performance. Although in the past few years many different techniques have been reported to reduce the spherical aberration effect, no optimum solution has been found. Here we concentrate on a technique whose main feature is its simplicity. We refer to the use of purely absorbing beam-shaping elements, which with a minimum modification of optical architecture will allow a significant reduction of the spherical aberration effect. Specifically, we will show that an adequately designed reversed-Gaussian aperture permits the production of a focal spot whose form changes very slowly with the spherical aberration.

OCIS codes: 220.1000, 140.3300, 180.1790, 210.0210, 140.7010.

1. INTRODUCTION

The search for strategies for reduction of the spherical aberration (SA) effect in the performance of optical instruments has been the aim of important research efforts, such as in the early work by Tsujiuchi,[1] where some methods for compensation of SA in paraxial imaging systems were analyzed, and in the work by Barakat and Houston,[2] where the SA-balancing relation is obtained for the case of annularly apertured paraxial imaging systems. More recently, and still within the context of paraxial imaging, the use of shaded[3–6] or phase[7] pupil apertures has been proposed for reduction of the SA influence. Although phase apertures are usually more appropriate than shaded apertures due to their higher light throughput, they have the drawback that their performance is strongly degraded when the illumination wavelength changes. In addition, they can produce null values in the optical transfer function for out-of-focus planes, which can be detrimental if *a posteriori* digital processing is required.

In recent years, and due mainly to the inception and development of laser sources, a revolution in optical instrumentation has occurred. Let us cite, for example, confocal scanning microscopy (CSM), which allows the production of sharp three-dimensional (3D) images from thick, usually biological, object structures.[8] Also noteworthy is the new generation of multilayer optical data storage (ODS) systems, which will allow a storage capacity greater than 50 GB on a disk.[9] Another interesting optical tool of recent development is laser trapping technology, which is now widely used in biology and scanning microscopy.[10] In these applications specimens are trapped and manipulated by sharply focused laser beams.

All three optical tools mentioned above have in common the following features: (a) the incident laser beam is tightly focused by a high-numerical-aperture (NA) objective and (b) the beam emerging from the objective focuses deeply through an interface between two media of different refractive index. Such a refractive index mismatch produces an important amount of SA, which strongly degrades the spatial resolution, in the case of CSM[11–14] and ODS[15] systems, or impoverishes the trapping power in the case of the laser trapping technology.[16] It is then clear that new strategies for reduction of the SA effect in high-NA optical instruments need be investigated.

Among the solutions reported for compensation of the SA effect, one of the most remarkable is the proposal of altering the tube length at which the objective is operated.[17–19] However, this technique does not provide a dynamic correction of the SA generated when scanning at different depths. On the other hand, altering the tube length produces higher orders of SA. Another solution, which indeed is commercially available in modern high-NA objectives, is the use of a correction collar to reduce the SA introduced due to the index mismatch. Note, however that, as stated in Ref. 20, the setting of the correction collar is often difficult due to the lack of quantitative criterion and problems caused by the focal shift introduced during the adjustment. An optimum solution to the SA compensation problem comes from the use of adaptive optics, which offers a versatile solution because it is able to adjust dynamically the correction for different depths

into the thick object structure.[21–23] However, the practical implementation of this technique is not an easy task.

Here we concentrate on another slightly less-efficient technique, but which is mainly featured by its simplicity. We refer to the use of purely absorbing beam-shaping elements, which with minimum modification of the optical architecture will allow a significant reduction of the SA effect. In the past few years the use of purely absorbing or complex-transmittance pupils has been extensively proposed to improve the resolution of high-NA scanning systems.[24–31] Here we will show that a purely absorbing radially symmetric pupil filter as inserted in the aperture stop of the high-NA objective can produce a focused spot that is highly insensitive to the variations of SA. Specifically, we will show that an adequately designed reversed Gaussian variation allows the production of a spot whose form changes very slowly with the SA.

2. BASIC THEORY

To describe our approach, we start by considering a high-NA objective lens that is illuminated by a monochromatic, scalar plane wave. In the simple scheme of Fig. 1, we represent the objective by a lens that has the aperture stop on its front focal plane. According to the scalar, nonparaxial Debye's formulation, which expresses the field after the lens as a superposition of plane waves, and assuming that the since condition holds, the amplitude distribution in the neighborhood of the focal point can be expressed as[32]

$$U(v,z_N)=\int_0^{\alpha}P(\theta)\sqrt{\cos\theta}J_0\left(kv\frac{\sin\theta}{\sin\alpha}\right)\exp[ikW(\theta)]\times\exp\left(-ikz_N\frac{\sin^2(\theta/2)}{\sin^2(\alpha/2)}\right)\sin\theta\,\mathrm{d}\theta. \quad (1)$$

In Eq. (1) $P(\theta)$ accounts for the amplitude transmittance at the objective exit pupil, and α is the maximum value for the aperture angle θ. Lateral and axial positions are expressed through normalized coordinates

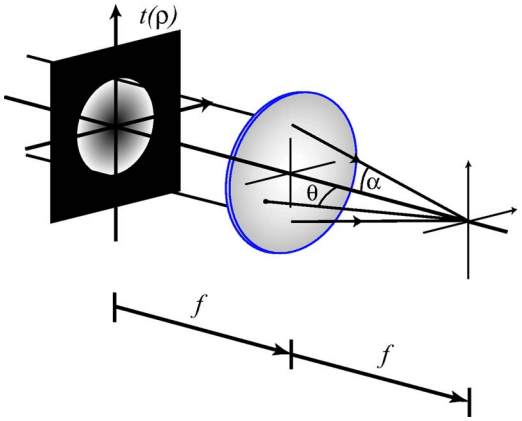

Fig. 1. Scheme of focusing by a high-NA telecentric objective lens.

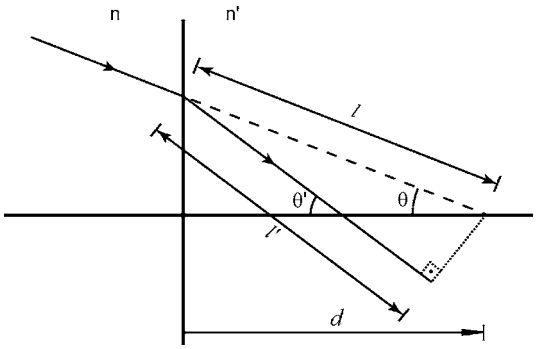

Fig. 2. Scheme for the evaluation of phase distortion introduced when a tightly focused light beam passes through a plane surface of refractive index step.

$$v=r\sin\alpha,\quad z_N=2z\sin^2\left(\frac{\alpha}{2}\right), \quad (2)$$

respectively, where r and z are cylindrical coordinates with origin at the focal point. We have included a phase factor, $W(\theta)$, which in the forthcoming analysis will account, in units of wave length, for the aberrations induced due to the index mismatch. Note that, according to the sine condition, the amplitude transmittance $t(\rho)$ at the aperture stop of the objective is related to the $P(\theta)$ function through the equations

$$P(\theta)=t(\rho),\quad \rho=\frac{\sin\theta}{\sin\alpha}, \quad (3)$$

where the radial coordinate at the aperture stop is normalized so that $\rho=1$ at its maximum radial extension.

Next, we evaluate the phase distortion introduced by the refractive index mismatch. To describe the field in the second material we assume that each plane-wave component of the field emerging from the objective obeys the refraction law when refracted at the interface. The resulting field is then reconstructed as the superposition of refracted plane waves. In Fig. 2 the plane waves are represented through a light ray normal to the plane wavefront. It has been shown elsewhere[12,13] that the phase delay suffered by a ray emerging from the lens with angle θ is given by

$$W(\theta)=n'l'-nl=d(n'\cos\theta'-n\cos\theta), \quad (4)$$

where we have taken into account the Snell refraction law $n\sin\theta=n'\sin\theta'$.

Following the reasoning of Sheppard and Cogswell,[11] we expand this expression into power series of $s=\sin(\theta/2)$, up to a fourth-order approximation. We obtain

$$W(\theta)=d(n'-n)\left[1+\frac{2n}{n'}s^2+2(n'+n)\frac{n^2}{n'^3}s^4+\cdots\right]. \quad (5)$$

In Eq. (5) we find a constant term, which will be neglected in the forthcoming analysis, a term in s^2, which accounts for the refractive defocus, and a term in s^4 that represents the primary SA.

The phase distortion induced by the index mismatch can then be introduced in the focused field equation in the following way:

$$U(v,z'_N;w_{40}) = \int_0^{\alpha} P(\theta)\sqrt{\cos\theta}J_0\left(kv\frac{\sin\theta}{\sin\alpha}\right) \times\exp\left\{ik\left[w_{40}\frac{\sin^4(\theta/2)}{\sin^4(\alpha/2)} - z'_N\frac{\sin^2(\theta/2)}{\sin^2(\alpha/2)}\right]\right\}\sin\theta\,\mathrm{d}\theta, \tag{6}$$

where the coefficients for the refractive defocus and the primary SA, as measured in units of wavelength, are

$$w_{20} = 2d(n'-n)\frac{n}{n'}\sin^2\left(\frac{\alpha}{2}\right),$$

$$w_{40} = 2d(n'^2-n^2)\frac{n^2}{n'^3}\sin^4\left(\frac{\alpha}{2}\right), \tag{7}$$

respectively. In addition, we have defined the reduced axial coordinate as $z'_N=z_N-w_{20}$. Note that Eq. (6) is essentially the equation deduced in Ref. 11. More accurate calculations should take into account the influence of the transmission coefficients of the interface.[33–35] However, the basic principle being presented here can be demonstrated without these coefficients. Further refinement of the method would require including these coefficients.

3. AXIAL INTENSITY DISTRIBUTION

Although Eq. (6) is a very compact formula, which allows the calculations of the spherically aberrated 3D focused field, it is difficult to extract from it any intuitive information that permits the development of methods for reduction of the SA effect. For that reason we prefer to work with a much simpler formula that provides only partial information of the field, but which will provide a powerful, simple mathematical tool to tackle the design of strategies for compensation of the SA effect. To this end, we first particularize Eq. (6) to points in the optical axis, and then perform the following nonlinear mapping:

$$\zeta = \frac{\sin^2(\theta/2)}{\sin^2(\alpha/2)} - 0.5, \quad q(\zeta) = P(\theta)\sqrt{\cos\theta}. \tag{8}$$

we obtain

$$U(v=0,z'_N;w_{40}) = \int_{-0.5}^{0.5} q(\zeta)\exp\left(i\frac{2\pi}{\lambda}w_{40}\zeta^2\right) \times\exp\left[-i\frac{2\pi}{\lambda}(z'_N-w_{40})\zeta\right]\mathrm{d}\zeta, \tag{9}$$

where some irrelevant constant factors have been omitted. The formula in Eq. (9) is similar to the classical one obtained by Ojeda-Castañeda *et al.*[4,5] in a paraxial context. Here we have shown that the same formula, but obtained through a much more general nonlinear mapping, can be applied to describe the focusing properties of high-NA scanning optical instruments. To illustrate this property, in Fig. 3 we show the axial intensity profiles corresponding to both low-NA (NA=0.1, air) and high-NA (NA=1.2, water) focusing elements with a clear circular aperture as the aperture stop and for increasing values of w_{40}. Note that in both cases the axial intensity profiles are not centered at $z'_N=0$, but are centered at the plane known as the best focal plane $z'_N=w_{40}$, as clearly expected from the kernel of the Fourier transformation in Eq. (9).[5] Note, however, that in the high-NA case the axial intensity profiles are not symmetric about that point. This is due to the $\sqrt{\cos\theta}$ factor that arises from the energy projection from a plane to the surface of a sphere, inherent in the fulfillment of the sine condition. In the high-NA case this factor is much more relevant than in the low-NA one.

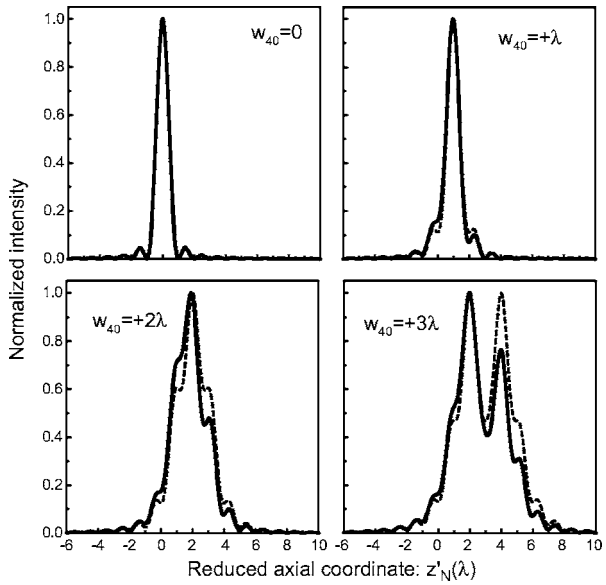

Fig. 3. Axial intensity profiles corresponding to a low-NA (dotted curves) and a high-NA (solid curves) focusing element with a clear circular aperture as the aperture stop and for increasing values of w_{40}. Since to perform the nonlinear mapping of Eqs. (7), the value of α must be known, in our calculations we assumed NA=0.1 (air) and NA=1.2 (water).

The above formulation constitutes a very useful tool for the analysis of the performance of the influence of SA in high-NA scanning optical instruments. What is more important, however, is that it provides us with a powerful tool for the design of beam-shaping strategies for reduction of the SA effect.

4. DESIGN OF BEAM-SHAPING ELEMENTS FOR REDUCTION OF THE SPHERICAL ABERRATION EFFECT

It has been known for many years that in a paraxial focusing regime, an aperture stop with Gaussian transmittance allows the production of a focused spot whose position and form change very slowly with the spherical aberration.[3] Note, however, that a Gaussian pupil is not a realistic solution for the SA problem in high-NA scanning optical instruments. This is because the Gaussian aperture is nothing more than a reduction of the effective NA of the objective lens, and it is a well-known fact that a lower-NA objective is much less sensitive to SA. To still profit from the abilities of Gaussian transmittances, but avoid the reductions in effective NA, we can make use of Eq. (9) and also of the concept of axial invariance of pupil

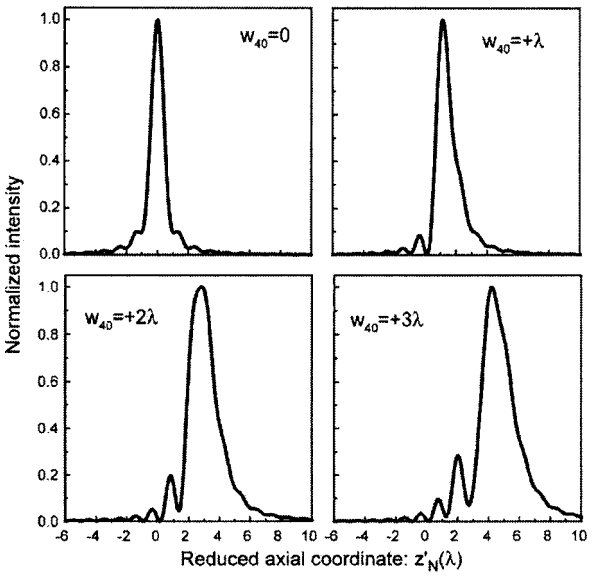

(a)

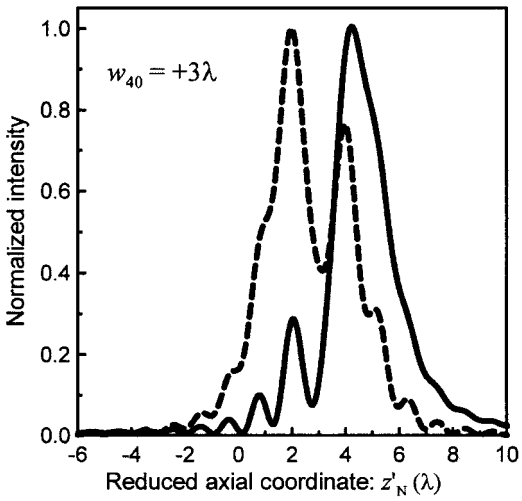

(b)

Fig. 4. (a) Axial intensity profiles corresponding to a high-NA focusing element with the reversed-Gaussian aperture as the aperture stop and for increasing values of w_{40}. In our calculations we considered the case $w=0.65$. (b) Intensity profiles produced by the circular aperture (dashed curve) and the reversed-Gaussian filter (solid curve) for $w_{40}=3\lambda$.

filters, reported by Campos and co-workers.[36] In that work, the authors established the general conditions that pupil filters must satisfy to produce an identical axial response. Specifically, we proceed in the following way. First we consider the Gaussian amplitude transmittance

$$t(\rho)=\exp[-(\rho/\omega)^2]. \tag{10}$$

This transmittance can be expressed in terms of the aperture angle, after performing the mapping $\rho=\sin\theta/\sin\alpha$, as

$$P(\theta)=\exp\left[-\left(\frac{\sin\theta}{\omega\sin\alpha}\right)^2\right]. \tag{11}$$

Then we calculate the function $Q(\zeta)$ by performing the nonlinear mapping of Eqs. (8):

$$Q(\zeta)=\exp\left\{-\frac{1-[\cos^2(\alpha/2)-2\zeta\sin^2(\alpha/2)]^2}{(\omega\sin\alpha)^2}\right\}. \tag{12}$$

Note that in this mapping we have not included the factor $\sqrt{\cos\theta}$. Finally we take into account that, as established in Ref. 36, an identical axial response, but an opposite transverse response, is produced by a pupil filter $\bar{Q}(\zeta)$ such that

$$\bar{Q}(\zeta)=Q(-\zeta). \tag{13}$$

Then we propose an amplitude transmittance in the form

$$\bar{t}(\rho)=\exp\left\{-\frac{1-[2\cos^2(\alpha/2)-\sqrt{1-\rho^2\sin^2\alpha}]^2}{\omega^2\sin^2\alpha}\right\}. \tag{14}$$

Next, in Fig. 4(a) we show the axial intensity profiles corresponding to a high-NA (NA=1.2 water) focusing element with the reversed-Gaussian aperture as the aperture stop and for increasing values of w_{40}. If we compare Fig. 4(a) with Fig. 3, we verify that degradation of the axial intensity as w_{40} increases has been reduced. Note that now the best focal plane is not at $z'_N=w_{40}$, but displaced toward higher values of z'_N.[37] A more detailed comparison is shown in Fig. 4(b), in which we compare the circular aperture with the reversed-Gaussian filter. As the figure of merit for the comparison, we have calculated the standard deviation on the axial intensity distributions, which is a measure of their effective width. The values of the standard deviation are 1.84 in the case of the circular aperture and 1.63 in the case of the reversed-Gaussian filter.

Naturally the focusing behavior of a high-NA optical instrument should be evaluated not only in terms of the axial behavior, but also in terms of the lateral profile of the point-spread function. Therefore, to illustrate the power of our proposal we have calculated the intensity distribution in the best focal plane for both cases: the cir-

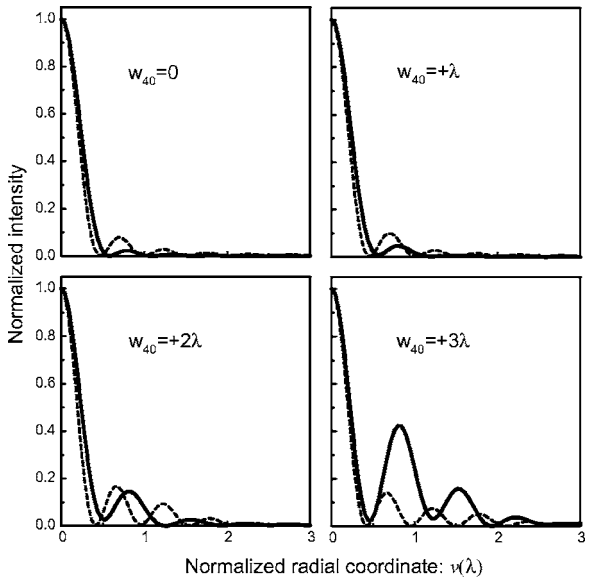

Fig. 5. Lateral responses corresponding to a high-NA focusing element with the circular (solid curve) or the reversed-Gaussian aperture (dashed curve) as the aperture stop and for increasing values of w_{40}.

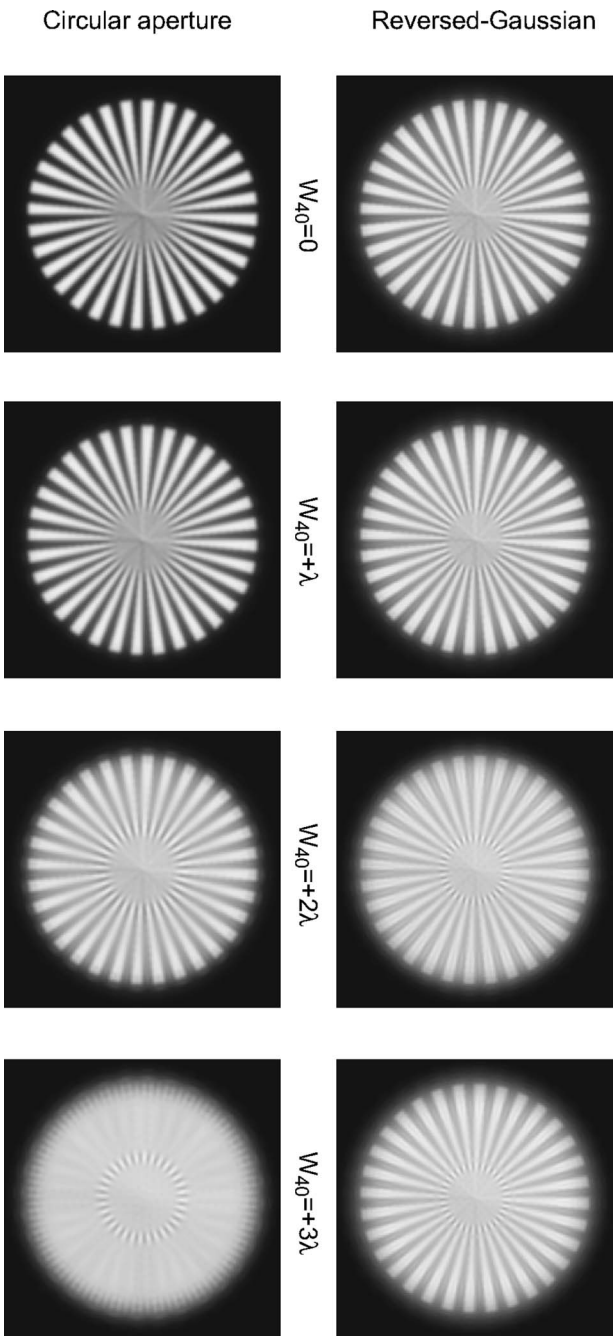

Fig. 6. Numerically evaluated images of a typical spoke target for increasing SA.

cular and the reversed-Gaussian aperture. As we see in Fig. 5, in the absence of SA the circular aperture produces, of course, slightly better results. However, as the SA increases, the response of the circular aperture degrades very fast, whereas the response of the reversed-Gaussian profile remains fairly stable.

Finally, to have a visual insight of the improvements obtained with the reversed-Gaussian aperture we have performed a numerical imaging experiment. We selected the spoke target as the synthetic object for the simulations. The target contains information from a very wide range of spatial frequencies. The images were obtained by 2D convolving the lateral responses in Fig. 5 with the target. The results are shown in Fig. 6. Note from Fig. 6 that in the absence of aberration the performance of the circular aperture is slightly better. However, the reversed-Gaussian aperture is much more robust against increasing SA. In other words, we can affirm that the reversed-Gaussian profile confers on the high-NA system an important tolerance to SA. This tolerance allows the high-NA optical instrument to have undegraded performance as it scans deeply into a medium of different refractive index.

5. CONCLUSIONS

In this paper we have obtained two important results. We have shown that the classical formula, obtained by Ojeda-Castañeda *et al.*[4] for a description of the influence of SA in focusing paraxial geometries, can be applied to a much more general situation. We refer to the focusing properties of high-NA scanning optical instruments. On the other hand, and on the basis of such a formula, we have tackled the design of beam-shaping elements for reduction of the SA effect. Specifically we have found that a reversed Gaussian aperture allows the production of a focused spot whose form changes very slowly with the amount of SA. The production of such elements can be easily done by use of annular binarizing techniques.[38] We have performed a simulation, with a spoke target as a synthetic object, that shows that the reversed-Gaussian profile confers on the high-NA system an important robustness against SA and that allows high-NA optical scanning instruments to have undegraded performance as they scan deeply into a medium of different refractive index.

ACKNOWLEDGMENTS

The authors acknowledge stimulating discussions with J. Ojeda-Castañeda (Universidad de Las Americas, México). We thank M. Kowalczyk (University of Warsaw, Poland) for some interesting suggestions concerning the bibliographic background. This work was funded by the Plan Nacional $I+D+I$ (grant DPI2003-4698), Ministerio de Ciencia y Tecnología. Isabel Escobar acknowledges the Ministerio de Educatión y Ciencia for a predoctoral grant.

Corresponding author Manuel Martínez-Corral's e-mail address is manuel.martinez@uv.es.

REFERENCES

1. T. Tsujiuchi, "Correction of optical images by compensation of aberrations and by spatial frequency filtering," Prog. Oceanogr. **2**, 133–180 (1963).
2. R. Barakat and A. Houston, "Transfer function of an annular aperture in the presence of spherical aberration," J. Opt. Soc. Am. **55**, 538–541 (1965).
3. J. P. Mills and B. J. Thompson, "Effect of aberrations and apodization on the performance of coherent optical systems. I. The amplitude impulse response," J. Opt. Soc. Am. A **3**, 694–703 (1986).
4. J. Ojeda-Castañeda, P. Andrés, and A. Diaz, "Annular apodizers for low sensitivity to defocus and to spherical aberration," Opt. Lett. **11**, 487–489 (1986).

5. J. Ojeda-Castañeda, P. Andrés, and A. Diaz, "Strehl ratio with low sensitivity to spherical aberration," J. Opt. Soc. Am. A **5**, 1233–1236 (1988).
6. J. Ojeda-Castañeda, E. Tepichin, and A. Pons, "Apodization of annular apertures: Strehl ratio," Appl. Opt. **27**, 5140–5145 (1988).
7. S. Mezouari and A. R. Harvey, "Phase pupil functions for reduction of defocus and spherical aberration," Opt. Lett. **28**, 771–773 (2003).
8. J. B. Pawley, ed., *Handbook of Biological Confocal Microscopy* (Plenum, 1995).
9. S. Stallinga, "Compact description of substrate-related aberrations in high numerical-aperture optical disk readout," Appl. Opt. **44**, 849–858 (2005).
10. A. Rohrbach and E. H. K. Stelzer, "Optical trapping of dielectric particles in arbitrary fields," J. Opt. Soc. Am. A **18**, 839–853 (2001).
11. C. J. R. Sheppard and C. J. Cogswell, "Effects of aberrating layers and the tube length on confocal imaging properties," Optik (Stuttgart) **87**, 34–38 (1991).
12. P. Török, P. Varga, Z. Laczik, and G. R. Booker, "Electromagnetic diffraction of light focused through a planar interface between materials of mismatched refractive indices: an integral representation," J. Opt. Soc. Am. A **12**, 325–332 (1995).
13. M. J. Booth, M. A. A. Neil, and T. Wilson, "Aberration correction for confocal imaging in refractive-index-mismatch media," J. Microsc. **192**, 90–98 (1998).
14. O. Haeberlé, "Focusing of light through a stratified medium: a practical approach for computing microscope point spread functions. Part II: Confocal and multiphoton microscopy," Opt. Commun. **235**, 1–10 (2004).
15. T. D. Lister, R. S. Upton, and H. Luo, "Objective lens design for multiple-layer optical data storage," Opt. Eng. **38**, 295–301 (1999).
16. A. Rohrbach and E. H. K. Stelzer, "Trapping forces, force constant, and potential depths for dielectric spheres in the presence of spherical aberrations," Appl. Opt. **41**, 2494–2507 (2002).
17. C. J. R. Sheppard and M. Gu, "Aberration compensation in confocal microscopy," Appl. Opt. **30**, 3563–3568 (1991).
18. P. C. Ke and M. Gu, "Characterization of trapping force in the presence of spherical aberration," J. Mod. Opt. **45**, 2159–2168 (1998).
19. S. N. S. Reihani, H. R. Khalesifard, and R. Golestanian, "Measuring lateral efficiency of optical traps: the effect of tube length," Opt. Commun. **259**, 204–211 (2006).
20. M. Schwertner, M. J. Booth, and T. Wilson, "Simple optimization procedure for objective lens correction collar setting," J. Microsc. **217**, 184–187 (2005).
21. M. J. Booth, M. A. A. Neil, R. Juskaitis, and T. Wilson, "Adaptive aberration correction in a confocal microscope," Proc. Natl. Acad. Sci. U.S.A. **99**, 5788–5792 (2002).
22. E. Theofanidou, L. Wilson, W. J. Hossak, and J. Artl, "Spherical aberration correction for optical tweezers," Opt. Commun. **236**, 145–150 (2004).
23. S. Somalinga, K. Dressbach, M. Hain, S. Stankovic, T. Tschudi, J. Knittel, and H. Richter, "Effective spherical aberration compensation by use of nematic liquid-crystal device," Appl. Opt. **43**, 2722–2729 (2004).
24. M. A. A. Neil, R. Juskaitis, T. Wilson, Z. J. Laczik, and V. Sarafis, "Optimized pupil–plane filters for confocal microscope point-spread function engineering," Opt. Lett. **25**, 245–247 (2000).
25. C. J. R. Sheppard, "Binary optics and confocal imaging," Opt. Lett. **24**, 505–506 (1999).
26. M. Martinez-Corral, M. T. Caballero, E. H. K. Stelzer, and J. Swoger, "Tailoring the axial shape of the point spread function using the Toraldo concept," Opt. Express **10**, 98–103 (2002).
27. C. M. Blanca and S. W. Hell, "Axial superresolution with ultrahigh aperture lenses," Opt. Express **10**, 893–898 (2002).
28. G. Boyer, "New class of axially apodizing filters for confocal scanning microscopy," J. Opt. Soc. Am. A **19**, 584–589 (2002).
29. M. Martinez-Corral, C. Ibáñez-López, G. Saavedra, and M. T. Caballero, "Axial gain in resolution in optical sectioning fluorescence microscopy by shaded-ring filters," Opt. Express **11**, 1740–1745 (2003).
30. S. S. Sherif and P. Török, "Pupil plane masks for super-resolution in high-numerical-aperture focusing," J. Mod. Opt. **51**, 2007–2019 (2004).
31. C. Ibáñez-López, G. Saavedra, G. Boyer, and M. Martínez-Corral, "Quasi-isotropic 3-D resolution in two-photon scanning microscopy," Opt. Express **12**, 6168–6174 (2005).
32. M. Gu, *Advanced Optical Imaging Theory* (Springer-Verlag, 2000).
33. C. J. R. Sheppard and P. Török, "Effects of specimen refractive index on confocal imaging," J. Microsc. **185**, 366–374 (1997).
34. P. Török and P. Varga, "Electromagnetic diffraction of light focused through a stratified medium," Appl. Opt. **36**, 2305–2312 (1997).
35. O. Haeberlé, M. Ammar, H. Furukawa, K. Tenjimbayashi, and P. Torok, "Point spread function of optical microscopes imaging through stratified media," Opt. Express **11**, 2964–2969 (2003).
36. J. Campos, J. C. Escalera, C. J. R. Sheppard, and M. J. Yzuel, "Axially invariant pupil filters," J. Mod. Opt. **47**, 57–68 (2000).
37. D. D. Lowenthal, "Maréchal intensity criteria modified for Gaussian beams," Appl. Opt. **13**, 2126–2133 (1974).
38. M. Martínez-Corral, L. Muñoz-Escriva, M. Kowalczyk, and T. Cichocki, "One-dimensional iterative algorithm for three-dimensional point-spread function engineering," Opt. Lett. **26**, 1861–1863 (2001).